Multi-MA Fusion Accelerator Performance Insensitivity to Electrode Contamination

Nathan P. Brown,* David C. Fairchild, Christopher A. Jennings, Leah N. Appelhans, Jacob T. Banasek, and Nichelle Bennett

Sandia National Laboratories, PO Box 5800, Albuquerque, New Mexico 87185-1189, USA

(Received 23 July 2026; revised 25 September 2026; accepted 8 October 2026; published 10 November 2026)

We provide experimental support for a recent kinetic model study [N. Bennett and D. Welch, Phys. Plasma **32** (2025)] that unexpectedly reported the insensitivity of a multi-MA pulsed power magneto-inertial confinement fusion target to the final power feed contaminant inventory. We measured a 1% difference between the peak current coupled to the target by a nominal high-inductance inner magnetically insulated transmission line (MITL) and the peak current coupled to the target by a contaminated inner MITL in 18 MA experiments on the Z Pulsed Power Facility. We contaminated the inner MITL by adding a net 25 layers of atoms to the anode and cathode current-carrying surfaces via self-assembled monolayer formation of octylphosphonic acid ($PO_3C_8H_{19}$) and verified the contaminant's presence and behavior via x-ray photoelectron spectroscopy, time-of-flight secondary ion mass spectrometry, and *in situ* streaked visible spectroscopy. Our findings reinforce the emerging MITL physics description gleaned from recent kinetic simulations, and our efforts provide a method for testing wall contaminant sensitivity that may be adapted for other plasma-facing applications.

DOI: 10.1103/hkpv-c3y7

Pulsed power accelerators compress electrical energy in space and time to conduct MA currents through physics targets on ns to μs timescales [1,2]. Their applications range from laboratory astrophysics [3–6] to high-pressure material studies [7–9], but one of their key functions is to drive magneto-inertial confinement fusion reactions [10]. A particularly well-studied concept is the magnetized liner inertial fusion (MagLIF) platform [11,12]: 20 MA experiments on the Z Pulsed Power Facility have demonstrated ion temperatures up to 3.1 keV and produced 10^{13} deuterium-deuterium neutrons [13]. Magnetohydrodynamic (MHD) simulations indicate that MagLIF operated on a proposed 60 MA accelerator [14] could produce deuterium-tritium yields as high as 100 MJ, achieving net facility gain [13].

The MagLIF fusion yield scales with the peak current delivered to the target according to $I_{\max}^6$ [15]. The platform's performance consequently depends on the transmission efficiency of the final power feed, an inner magnetically insulated transmission line (MITL) that is subjected to MV/cm electric fields and >100 MA/cm^2 current densities. These extreme electromagnetic stresses source plasmas that shunt current from the load, reducing the MITL efficiency [16,17]. As the plasmas are seeded by neutral particles desorbed from the electrode surfaces, the pulsed power community has traditionally hypothesized that $I_{\max}$ is strongly coupled to the inner MITL surface contaminant inventory [18,19].

However, a recent kinetic simulation effort [20] unexpectedly observed that computationally varying the neutral inventory of the electrode surfaces in a high-inductance MagLIF inner MITL made virtually no impact on the target current coupling efficiency. In this paper, we report our experimental assessment of that prediction and our observed confirmation of its validity. Our findings challenge a long-standing hypothesis and support the physics picture emerging from contemporary power flow models.

The Z Facility sources a μs current pulse from an outer ring of Marx generator capacitor banks, shortens the pulse to a ∼100 ns rise time through a pulse-forming section, and then delivers the pulse to a MagLIF target through a radial 304L stainless steel (SS) vacuum-insulated MITL architecture [2]. The MITL architecture comprises a stacked set of four large-radius transmission lines that are combined into a single small-radius inner MITL feed by a post-hole convolute (PHC). The inner MITL comprises an anode and a cathode that are separated by a vacuum gap and are electrically connected through the MagLIF target.

The prevailing inner MITL physics description comes from a series of recent efforts [17,21,22] that employed the fully relativistic CHICAGO [23] particle-in-cell code to

*Contact author: npbrown@sandia.gov

Published by the American Physical Society under the terms of the Creative Commons Attribution 4.0 International license. Further distribution of this work must maintain attribution to the author(s) and the published article's title, journal citation, and DOI.

kinetically model the transmission line environment. The early-time electric field established across the MITL gap strips electrons from the cathode in a space-charge-limited manner. The current subsequently establishes a >100 T confining magnetic field while also rapidly heating the electrodes >1000 K in a few ns, desorbing neutral species that are quickly ionized. The resulting $>10^{19}$ cm^{-3} plasmas are largely confined near the electrode surfaces, but instability-driven transport [24] enables a fraction of these surface plasmas to drift into the gap where they form a lower-density ($<10^{18}$ cm^{-3}) gap plasma.

The gap plasma mediates charged particle transport via a Hall-related mechanism, shunting current through the gap and away from the MagLIF target in a manner that scales as

$$j \sim \frac{nE}{B}, \tag{1}$$

where j is the loss current density, n is the plasma density, E is the average electric field across the gap, and B is the average magnetic field in the gap [21]. The current lost in the inner MITL is limited by the gap plasma density, so, because the gap plasma is sourced by the surface plasma, which, in turn, is seeded by electrode surface contaminants, a reasonable strategy for maximizing the delivered current is to minimize the electrode contaminant inventory. For this reason, Z hardware are routinely cleaned, hydrogen-fired, and stored in dry gas purge boxes.

The recent CHICAGO simulation effort [20] noted above, however, reported ≤2% change in the peak current delivered through a high-inductance MagLIF inner MITL as the contaminant inventory was increased from a nominal 8.3 monolayers (ML) to a heightened 32 ML (with 1 ML defined as 10^{15} H_2O molecules/cm^2). The authors further reported that decreasing the inventory to approximately 1 ML only increased the peak current by 5% compared to nominal.

The simulations found that increasing the neutral inventory indeed increased the surface plasma density but did not observe this to significantly alter the gap plasma characteristics. Instead, due to the strong magnetic confinement and concomitant reduction in the electric field penetration with density, the higher-density plasma remained confined to the electrode surfaces and consequently did not participate in the current loss.

This unexpected finding offers an opportunity to assess the physics description provided by the body of modern kinetic modeling efforts. We tested the prediction by comparing the current delivered to a MagLIF target in back-to-back synchronous-discharge 80 kV experiments on Z: one in which we employed a nominal inner MITL and one in which we contaminated the inner MITL by functionalizing the anode and cathode current-carrying surfaces with a single molecular monolayer of octylphosphonic acid ($PO_3C_8H_{19}$).

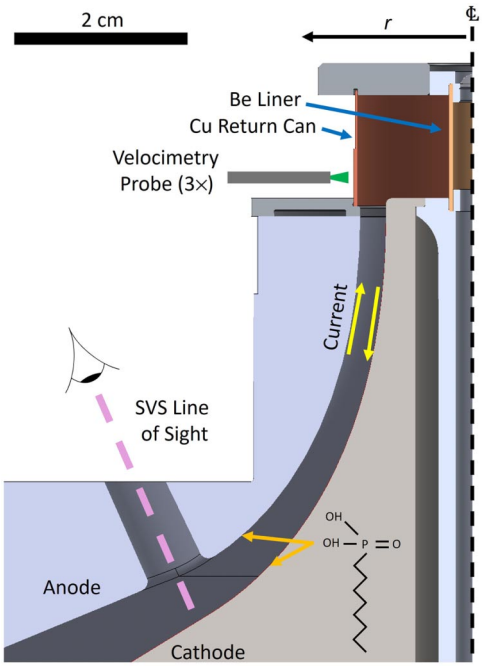


FIG. 1. Half cross section of the inner MITL and MagLIF target region. The radius is measured from the marked center line. Lossy plasma sourced from the electrode surfaces enters the vacuum gap between the anode and cathode and between the return can and liner.

Figure 1 shows a simplified half cross section of the high-inductance inner MITL and associated MagLIF target used in these experiments [25]. Though we employed a standard MagLIF target geometry (including the Be liner), because our primary objective was to measure current delivery to the target and not to measure a fusion yield, we simplified the experiment by omitting the fuel, external field coils, and laser preheat. We employed photonic Doppler velocimetry [26,27] with a 2 GHz upshift and the velocity interferometer system for any reflector [28,29] with velocity-per-fringe values of 309.7, 510.9, and 828.8 m/s to measure the return can explosion velocities at the axial location shown in Fig. 1 with three probes separated by 120° about the azimuth. We employed streaked visible spectroscopy (SVS) [30] to characterize the inner MITL plasma through the anode hole shown in Fig 1. We carefully positioned and designed the anode hole with MHD simulations to avoid perturbing the current flow to the target.

We measured the current delivered to the target by computationally unfolding the surface velocity measurements with a custom version of the GORGON Eulerian resistive MHD code [31–33] that we adapted to simulate magnetically driven fusion experiments on Z [33–36]. Assuming the return can surface expansion is driven solely by the magnetic pressure generated by the load current, we iteratively optimized a candidate current waveform seeded by larger-radius B-dot measurements [30] until

the computed velocities matched those measured in the experiment [37]. As an accurate current inference requires a well-constrained high-pressure equation of state (EOS) and electrical conductivity (ECON), we measured the velocity of a Cu surface for which we could employ the well-established SESAME 3325 EOS and 29235 ECON tables [38] in our unfolds.

The primary constituents of pulsed power contamination are traditionally hypothesized to be H_2, H_2O, and small hydrocarbons weakly bonded to the electrode surfaces and H entrained in the near-surface SS bulk [19,22]. A previous SVS study in the Z PHC region confirmed the late-time presence of various forms of hydrogen and carbon and hypothesized the presence of oxygen [16]. We, therefore, chose to contaminate the surfaces with a single layer of $PO_3C_8H_{19}$ to add a relevant, controlled number of atomic layers comprising primarily H, O, and C in a uniform manner over a large surface area that would enable the contamination layer to remain bonded to the surfaces under vacuum.

After applying standard Z cleaning and hydrogen-firing treatments, we functionalized the gap-facing anode and cathode surfaces below the return can to a radius (r) of 5.5 cm via self-assembled monolayer formation (SAM) [39]. We plasma-cleaned the surfaces, soaked the electrodes in an octylphosphonic acid solution in ethanol (100 mM) for 1 week, and then dried them at 100 °C in an oven overnight. We finally sonicated the samples in ethanol and then water to remove any unbound residues. Though $PO_3C_8H_{19}$ comprises 31 atoms, the binding process results in a net loss of two water molecules from the surface for a net addition of 25 atoms per $PO_3C_8H_{19}$ molecule.

Prior work [40,41] has shown that the treatment of 316L SS with alkyl phosphonic acids results in robust SAMs, with single molecular monolayer formation confirmed by x-ray photoelectron spectroscopy (XPS), surface contact angle measurements, and atomic force microscopy characterization of surface roughness before and after functionalization. We checked for successful functionalization of 304L SS by examining the surfaces of functionalized 304L SS coupons at multiple locations via XPS and time-of-flight secondary ion mass spectrometry (ToF-SIMS) and comparing the measurements to those taken of nominal 304L SS coupons. XPS observed the presence of P and the heightened presence of C and O above standard values (XPS is insensitive to H), indicating successful functionalization and survivability in high vacuum. ToF-SIMS confirmed the presence of a molecule with the expected mass-to-charge ratio. Results from efforts investigating aminopropylsilane on 316L SS [41] and octyldecylphosphonic acid on metal oxide surfaces (TiO_2 and Al_2O_3) [42] lead us to estimate that the areal density of the $PO_3C_8H_{19}$ on a smooth 304L SS surface is on the order of $1/3 \times 10^{15}$ cm^{-2}.

The computational definition of a contaminant monolayer cited from the motivating simulation study [20] stems from an assumed smooth-surface H_2O-only contaminant areal density of 10^{15} particles/cm^2. The justification for assigning the nominal MITL inventory as 8.3 ML (rather than 1 ML) has previously been provided by the need to apply a plausible surface roughness factor [21,43]. Because the functionalized $PO_3C_8H_{19}$ contains $\sim 8\times$ as many atoms as H_2O and was added at $\sim 1/3$ the assumed density, we estimate that our surface contamination method provides an inventory multiplier of $1 + 8f/3$ where f is the fractional surface roughness factor compared to the nominal contaminant species. If $f = 1$ and the nominal inventory is 8.3 ML, for example, the total contaminant inventory on a functionalized surface is on the order of 30 ML.

Joule heating calculations [22] show that the inner MITL surface temperature increases from the initial desorption threshold of weakly bonded atoms to the steel surface melt threshold in ~5 ns, so the precise binding energy of octylphosphonic acid to the steel has little impact on its desorption characteristics. CHICAGO simulations [22] indicate that the extreme inner MITL electromagnetic conditions, which produce gap plasma electron temperatures exceeding 100 eV, rapidly fully dissociate and ionize any desorbed species. However, given the size of $PO_3C_8H_{19}$ compared to the molecules traditionally believed to reside on the MITL surfaces, we fielded SVS in the inner MITL as a check for the presence of unintended molecular signatures arising from incompletely dissociated $PO_3C_8H_{19}$.

Figure 2 compares the average velocities measured in the two experiments, alongside their associated inferred

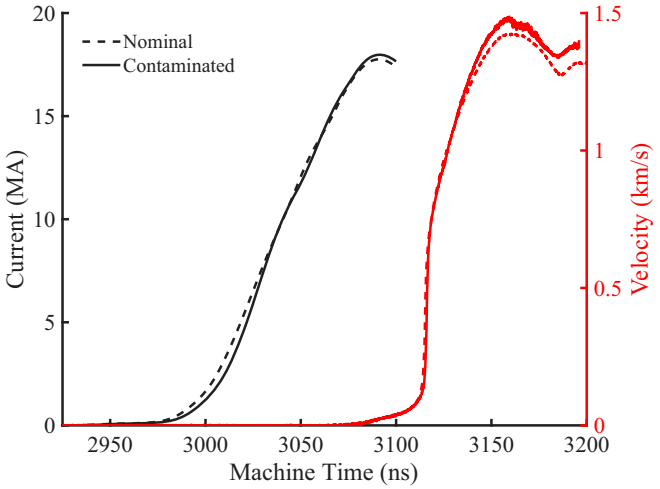


FIG. 2. Comparison of the target currents measured in the nominal and contaminated MITL experiments, alongside the accompanying surface velocity measurements. The measured peak currents differ by 1%. The contaminated experiment traces are shifted −4 ns to facilitate the comparison.

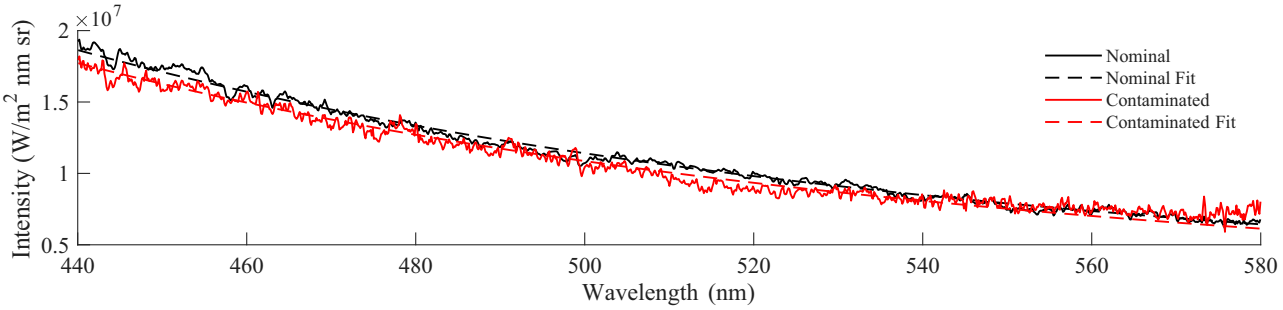


FIG. 3. Comparison of the intensity-calibrated SVS spectra integrated across 3025–3035 ns measured in the nominal and contaminated MITL experiments. Also shown are the respective Planckian fits. The lack of line absorption supports the contaminant surrogacy.

target currents. The contaminated shot traces are shifted −4 ns to compensate for shot-to-shot timing jitter to better facilitate the comparisons. Of the 25 MA peak current delivered to the outer MITL stack, we measured a peak current at the target of 17.8 MA in the nominal experiment and 18.0 MA in the contaminated experiment. As the peak currents differ by just 1%, the results support the CHICAGO prediction.

Figure 3 compares the broadband (440–580 nm) intensity-calibrated SVS spectra integrated across the earliest time window for which we collected sufficient signal above noise (3025–3035 ns), alongside their respective Planckian fits. Neither spectrum features discernible absorption lines, indicating that we measured continuum emission. Additional spectra collected across 650–680 nm also do not exhibit early-time line absorption. The inferred blackbody temperature from the Planckian fits is on the order of 10 eV for both experiments.

The SVS line of sight crosses through the low-density gap plasma and terminates at the high-density cathode surface plasma, where the blackbody temperature is inferred. PrismSPECT [44] spectral simulations with the octylphosphonic acid's atomic constituents and model-predicted gap plasma electron temperature, back-illuminated by the cathode surface plasma, predict that the gap plasma imprints no absorption lines on the continuum. Our spectra's agreement with this prediction, with specific emphasis on our lack of observation of molecular signals in the contaminated experiment, comports with the predicted $PO_3C_8H_{19}$ surrogacy.

Our work provides experimental evidence for a non-intuitive pulsed power current transmission prediction and thereby supports the physical picture constructed from CHICAGO simulations. It bolsters confidence in the use of kinetic models to both design multi-MA fusion experiments and to target contamination removal efforts. Though the current delivered in this experiment does not exhibit strong sensitivity to heightened inner MITL contamination, other geometries or electrode regions, including the MagLIF PHC, are predicted to exhibit greater contamination sensitivities and may therefore be better candidates for surface treatment efforts [20].

Pulsed power's focus on wall contamination is shared by a large range of plasma-facing applications, including magnetic confinement fusion [45] and semiconductor processing [46]. Our efforts provide a path for adding specific contaminant species in a well-controlled manner that may be adapted for understanding contaminant impacts and assessing cleaning protocols in some of these devices. Surface functionalization of a single molecular monolayer is a precise technique applicable to a large area whose effectiveness can be measured prior to the experiment and whose surrogacy can be both computationally and experimentally evaluated on an application-specific basis.

We thank the Z operations team for executing the experiments, Beth Willneff for performing the XPS measurements, Tony Ohlhausen for performing the ToF-SIMS measurements, and Mike Cuneo for his insightful comments. Sandia National Laboratories is a multimission laboratory managed and operated by National Technology & Engineering Solutions of Sandia, LLC, a wholly owned subsidiary of Honeywell International Inc., for the U.S. Department of Energy's National Nuclear Security Administration under Contract No. DE-NA0003525. This paper describes objective technical results and analysis. Any subjective views or opinions that might be expressed in the paper do not necessarily represent the views of the U.S. Department of Energy or the U.S. Government.

DATA AVAILABILITY

There are no publicly available research data or software supporting this manuscript. Requests for further information or data should be sent to the authors.

[1] J. Lehr and P. Ron, *Foundations of Pulsed Power Technology* (IEEE Press, Piscataway, NJ, USA, 2017).

[2] D. Sinars, M. Sweeney, C. Alexander, D. Ampleford, T. Ao, J. Apruzese, C. Aragon, D. Armstrong, K. Austin, T. Awe *et al.*, *Review of pulsed power-driven high energy density physics research on Z at Sandia*, Phys. Plasma **27**, 070501 (2020).

[3] J. E. Bailey, T. Nagayama, G. P. Loisel, G. A. Rochau, C. Blancard, J. Colgan, P. Cosse, G. Faussurier, C. J. Fontes, F. Gilleron *et al.*, *A higher-than-predicted measurement of iron opacity at solar interior temperatures*, Nature (London) **517**, 56 (2015).

[4] G. P. Loisel, J. E. Bailey, D. A. Liedahl, C. J. Fontes, T. R. Kallman, T. Nagayama, S. B. Hansen, G. A. Rochau, R. C. Mancini, and R. W. Lee, *Benchmark experiment for photoionized plasma emission from accretion-powered x-ray sources*, Phys. Rev. Lett. **119**, 075001 (2017).

[5] R. Datta, K. Chandler, C. Myers, J. Chittenden, A. Crilly, C. Aragon, D. Ampleford, J. Banasek, A. Edens, W. Fox *et al.*, *Plasmoid formation and strong radiative cooling in a driven magnetic reconnection experiment*, Phys. Rev. Lett. **132**, 155102 (2024).

[6] G. Loisel, J. Bailey, T. Nagayama, S. Hansen, G. Dunham, P. Gard, A. Colombo, A. Edens, R. Speas, Q. Looker *et al.*, *First measurement of Z opacity sample evolution near solar interior conditions using time-resolved spectroscopy*, Phys. Rev. Lett. **134**, 095101 (2025).

[7] M. D. Knudson, M. P. Desjarlais, and D. H. Dolan, *Shock-wave exploration of the high-pressure phases of carbon*, Science **322**, 1822 (2008).

[8] M. D. Knudson, M. P. Desjarlais, A. Becker, R. W. Lemke, K. R. Cochrane, M. E. Savage, D. E. Bliss, T. R. Mattsson, and R. Redmer, *Direct observation of an abrupt insulator-to-metal transition in dense liquid deuterium*, Science **348**, 1455 (2015).

[9] D. Fratanduono, M. Millot, D. Braun, S. Ali, A. Fernandez-Pañella, C. Seagle, J.-P. Davis, J. Brown, Y. Akahama, R. Kraus *et al.*, *Establishing gold and platinum standards to 1 terapascal using shockless compression*, Science **372**, 1063 (2021).

[10] *Prospects for low cost fusion development*, JASON, Technical Report No. JSR-18-011, 2018.

[11] S. A. Slutz and R. A. Vesey, *High-gain magnetized inertial fusion*, Phys. Rev. Lett. **108**, 025003 (2012).

[12] M. R. Gomez, S. A. Slutz, A. B. Sefkow, D. B. Sinars, K. D. Hahn, S. B. Hansen, E. C. Harding, P. F. Knapp, P. F. Schmit, C. A. Jennings *et al.*, *Experimental demonstration of fusion-relevant conditions in magnetized liner inertial fusion*, Phys. Rev. Lett. **113**, 155003 (2014).

[13] M. Gomez, S. Slutz, C. Jennings, A. Harvey-Thompson, M. Weis, W. Lewis, B. Hutsel, D. Lamppa, M. Geissel, J. Crabtree *et al.*, *Magnetized liner inertial fusion platform development to assess performance scaling with drive parameters*, Phys. Plasma **32**, 032702 (2025).

[14] W. Stygar, T. Awe, J. Bailey, N. Bennett, E. Breden, E. Campbell, R. Clark, R. Cooper, M. Cuneo, J. Ennis *et al.*, *Conceptual designs of two petawatt-class pulsed-power accelerators for high-energy-density-physics experiments*, Phys. Rev. ST Accel. Beams **18**, 110401 (2015).

[15] D. Ruiz, P. Schmit, D. Yager-Elorriaga, M. Gomez, M. Weis, C. Jennings, A. Harvey-Thompson, P. Knapp, S. Slutz, D. Ampleford *et al.*, *Exploring the parameter space of MagLIF implosions using similarity scaling. II. Current scaling*, Phys. Plasma **30**, 032708 (2023).

[16] M. R. Gomez, R. M. Gilgenbach, M. E. Cuneo, C. A. Jennings, R. D. McBride, E. M. Waisman, B. T. Hutsel, W. A. Stygar, D. V. Rose, and Y. Maron, *Experimental study of current loss and plasma formation in the Z machine post-hole convolute*, Phys. Rev. Accel. Beams **20**, 010401 (2017).

[17] N. Bennett, D. R. Welch, C. A. Jennings, E. Yu, M. H. Hess, B. T. Hutsel, G. Laity, J. K. Moore, D. V. Rose, K. Peterson *et al.*, *Current transport and loss mechanisms in the Z accelerator*, Phys. Rev. Accel. Beams **22**, 120401 (2019).

[18] M. E. Cuneo, P. R. Menge, D. L. Hanson, W. E. Fowler, M. A. Bernard, G. R. Ziska, A. B. Filuk, T. D. Pointon, R. A. Vesey, D. R. Welch *et al.*, *Results of vacuum cleaning techniques on the performance of LiF field-threshold ion sources on extraction applied-B ion diodes at 1-10 TW*, IEEE Trans. Plasma Sci. **25**, 229 (1997).

[19] M. E. Cuneo, *The effect of electrode contamination, cleaning and conditioning on high-energy pulsed-power device performance*, IEEE Trans. Dielectr. Electr. Insul. **6**, 469 (1999).

[20] N. Bennett and D. R. Welch, *Modeled sensitivity of multi-MA accelerator performance to electrode contaminant inventory*, Phys. Plasma **32**, 062702 (2025).

[21] N. Bennett, D. R. Welch, G. Laity, D. V. Rose, and M. E. Cuneo, *Magnetized particle transport in multi-MA accelerators*, Phys. Rev. Accel. Beams **24**, 060401 (2021).

[22] N. Bennett, D. R. Welch, K. Cochrane, K. Leung, C. Thoma, M. E. Cuneo, and G. Frye-Mason, *Electrode plasma formation and melt in Z-pinch accelerators*, Phys. Rev. Accel. Beams **26**, 040401 (2023).

[23] D. Rose, D. Welch, E. Madrid, C. Miller, R. Clark, W. Stygar, M. Savage, G. Rochau, J. Bailey, T. Nash *et al.*, *Three-dimensional electromagnetic model of the pulsed-power Z-pinch accelerator*, Phys. Rev. Spec. Top. Accel. Beams **13**, 010402 (2010).

[24] D. R. Welch, T. C. Genoni, C. Thoma, A. Russell, W. A. Stygar, K. K. Tummel, K. Beckwith, J. H. Hammer, and N. Bennett, *Electrode plasma transport into the gap of high-current Z-pinch accelerators*, Phys. Rev. Accel. Beams **29**, 093301 (2026).

[25] S. A. Slutz, M. C. Herrmann, R. A. Vesey, A. B. Sefkow, D. B. Sinars, D. C. Rovang, K. J. Peterson, and M. E. Cuneo, *Pulsed-power-driven cylindrical liner implosions of laser preheated fuel magnetized with an axial field*, Phys. Plasma **17**, 056303 (2010).

[26] O. T. Strand, D. R. Goosman, C. Martinez, T. L. Whitworth, and W. W. Kuhlow, *Compact system for high-speed velocimetry using heterodyne techniques*, Rev. Sci. Instrum. **77**, 083108 (2006).

[27] D. H. Dolan, *Extreme measurements with photonic Doppler velocimetry (PDV)*, Rev. Sci. Instrum. **91**, 051501 (2020).

[28] L. M. Barker and R. E. Hollenbach, *Laser interferometer for measuring high velocities of any reflecting surface*, J. Appl. Phys. **43**, 4669 (1972).

[29] D. H. Dolan, *Foundations of VISAR analysis*, Sandia National Laboratories, Technical Report No. SAND2006-1950, 2006.

[30] T. J. Webb, D. E. Bliss, G. A. Chandler, D. H. Dolan, G. Dunham, A. Edens, E. Harding, M. D. Johnston, M. C. Jones, S. Langendorf *et al.*, *Radiation, optical, power flow, and electrical diagnostics at the Z facility: Layout and techniques utilized to operate in the harsh environment*, Rev. Sci. Instrum. **94**, 031102 (2023).

[31] J. P. Chittenden, S. V. Lebedev, C. A. Jennings, S. N. Bland, and A. Ciardi, *X-ray generation mechanisms in three-dimensional simulations of wire array Z-pinches*, Plasma Phys. Controlled Fusion **46**, B457 (2004).

[32] A. Ciardi, S. V. Lebedev, A. Frank, E. G. Blackman, J. P. Chittenden, C. Jennings, D. J. Ampleford, S. Bland, S. C. Bott, J. Rapley *et al.*, *The evolution of magnetic tower jets in the laboratory*, Phys. Plasma **14**, 056501 (2007).

[33] C. A. Jennings, M. E. Cuneo, E. M. Waisman, D. B. Sinars, D. J. Ampleford, G. R. Bennett, W. A. Stygar, and J. P. Chittenden, *Simulations of the implosion and stagnation of compact wire arrays*, Phys. Plasma **17**, 092703 (2010).

[34] C. A. Jennings, J. P. Chittenden, M. E. Cuneo, W. A. Stygar, D. J. Ampleford, E. M. Waisman, M. Jones, M. E. Savage, K. R. LeChien, and T. C. Wagoner, *Circuit model for driving three-dimensional resistive MHD wire array Z-pinch calculations*, IEEE Trans. Plasma Sci. **38**, 529 (2010).

[35] T. J. Awe, C. A. Jennings, R. D. McBride, M. Cuneo, D. Lamppa, M. Martin, D. Rovang, D. Sinars, S. Slutz, A. Owen *et al.*, *Modified helix-like instability structure on imploding Z-pinch liners that are pre-imposed with a uniform axial magnetic field*, Phys. Plasma **21**, 056303 (2014).

[36] C. A. Jennings, D. J. Ampleford, D. C. Lamppa, S. B. Hansen, B. Jones, A. J. Harvey-Thompson, M. Jobe, T. Strizic, J. Reneker, G. Rochau *et al.*, *Computational modeling of krypton gas puffs with tailored mass density profiles on Z*, Phys. Plasma **22**, 056316 (2015).

[37] C. E. Myers, D. E. Bliss, P. M. Celliers, P. S. Datte, M. H. Hess, C. A. Jennings, M. C. Jones, D. J. Ampleford, C. R. Aragon, K. N. Austin *et al.*, *Spatially resolved measurements of load current delivery on a 14 ma, 100 ns pulsed power experiment using a line-imaging velocity interferometer*, Phys. Rev. Accel. Beams **26**, 070401 (2023).

[38] K. R. Cochrane, R. W. Lemke, Z. Riford, and J. H. Carpenter, *Magnetically launched flyer plate technique for probing electrical conductivity of compressed copper*, J. Appl. Phys. **119**, 105902 (2016).

[39] D. K. Schwartz, *Mechanisms and kinetics of self-assembled monolayer formation*, Annu. Rev. Phys. Chem. **52**, 107 (2001).

[40] A. Raman, M. Dubey, I. Gouzman, and E. S. Gawalt, *Formation of self-assembled monolayers of alkylphosphonic acid on the native oxide surface of ss316l*, Langmuir **22**, 6469 (2006).

[41] M. Kosian, M. M. J. Smulders, and H. Zuilhof, *Structure and long-term stability of alkylphosphonic acid monolayers on SS316l stainless steel*, Langmuir **32**, 1047 (2016).

[42] W. Gao, L. Dickinson, C. Grozinger, F. G. Morin, and L. Reven, *Self-assembled monolayers of alkylphosphonic acids on metal oxides*, Langmuir **12**, 6429 (1996).

[43] M. Li and H. F. Dylla, *Model for the outgassing of water from metal surfaces*, J. Vac. Sci. Technol. A **11**, 1702 (1993).

[44] I. E. Golovkin, M. F. Gu, J. J. MacFarlane, J. Sebald, and T. Walton, *Collisional-radiative spectral analysis code* PRISM-SPECT, High Energy Density Phys. **58**, 101255 (2026).

[45] J. Winter, *Wall conditioning in fusion devices and its influence on plasma performance*, Plasma Phys. Controlled Fusion **38**, 1503 (1996).

[46] V. M. Donnelly and A. Kornblit, *Plasma etching: Yesterday, today, and tomorrow*, J. Vac. Sci. Technol. A **31**, 050825 (2013).